
Article:
Mao, M, Zhang, L, Yang, L et al. (3 more authors) (2020) MPPT using modified salp swarm algorithm for multiple bidirectional PV-Ćuk converter system under partial shading and module mismatching. Solar Energy, 209. pp. 334-349. ISSN 0038-092X

https://doi.org/10.1016/j.solener.2020.08.078

MPPT Using Modified Salp Swarm Algorithm for Multiple Bidirectional PV-Ćuk Converter System under Partial Shading and Module Mismatching

Mingxuan Mao[1,2,*], Li Zhang[3], Lei Yang[4], Benjamin Chong[3], Han Huang[5], Lin Zhou[2]

[1]Postdoctoral Station of Electrical Engineering, Chongqing University, Chongqing 400044, China

[2] School of Electrical Engineering, Chongqing University, Chongqing 400044, China

[3]School of Electronic and Electrical Engineering, University of Leeds, Leeds LS2 9JT, United Kingdom

[4]Electric Power Research Institute of Yunnan Power Grid Co. Ltd., Kunming 650217, China

[5]Energy Safety Research Institute, Swansea University, Swansea SA1 8EN, Wales, United Kingdom

Abstract: This paper presents a configuration scheme based multiple bidirectional Ćuk converter with a modified salp swarm algorithm (SSA) based maximum power point tracking (MPPT) for photovoltaic (PV) system under partial shading and module mismatching. The proposed scheme is made up of multiple bidirectional PV-Ćuk converter (PVCC) modules in a series chain, a novel SSA with dynamic nonlinear w factor (DWSSA) based the distributed maximum power point tracking (MPPT) and a terminal step-up converter for load connection. First of all, the configuration offers the advantage that the PVCC provides a current by pass and can also be controlled to allow two PV panels in the module to track their available maximum power under partial shading or module mismatching. In addition, the DWSSA-MPPT control scheme is used to estimate the voltages corresponding to the maximum power each PV panel can generate under its specific weather conditions. Moreover, a state space model is developed for the PVCC and experimentally validated, and the control strategy for a PV system having more than one PVCC is discussed. Finally, a simulated PV system based the proposed configuration scheme is set up and results are analyzed, which demonstrates that compared with some existing algorithms, the scheme with DWSSA-MPPT method can highly be effective under partial shading and module mismatching.

Keywords: Multiple PV-Ćuk Converter (PVCC); Maximum Power Point Tracking (MPPT); Salp Swarm Algorithm (SSA); Photovoltaic (PV) System; under Partial Shading and Module Mismatching

1. Introduction

The issue of partial shading in PV power generation systems has been well-investigated by many researchers (Bingöl and Özkaya, 2018; Belhachat and Larbes, 2019; Mohamed et al., 2019; Tatabhatla et al., 2019; Yang al., 2019; Mao et al., 2020; Mirza et al., 2020). A standard solution has involved incorporating bypass diodes within the PV array, but it has been

recognized that this scheme alone reduces the power generated by the system (Boztepe et al., 2013; Gallardo-Saavedra and Karlsson, 2018; Munoz et al., 2011; Woyte et al., 2003).

Since the cost of power switching devices is steadily falling, the current trend is to replace the bypass diodes with power electronic converters, so that all series connected panels in an array can generate power corresponding to their respective levels of irradiation. Many such schemes have been proposed, based on either continuous or differential power processing approaches (Walker and Sernia, 2004; Upadhyay and Kumar, 2019; Hossain et al., 2018; Bratcu et al., 2010; Femia et al., 2008; Noguchi et al., 2002; Urtasun and Lu, 2015; Du and Lu, 2011; Kadri et al., 2011; Mao et al., 2018). An example of the former is illustrated where one or several series and/or parallel chained PV panels are connected to a DC-DC converter forming a PV and converter integrated module (Upadhyay et al., 2019; Zhuang et al., 2019; Ghaderi, 2019; Amir et al., 2019; Chen et al., 2019; Verdugo et al., 2019; Babu and Narasimharaju, 2020; Zhang et al., 2020; Alharbi et al., 2020). Connecting multiples of such modules in series can raise the voltage levels sufficiently to enable transformer-less grid connection. Several well-known DC-DC converter topologies have been considered for such a scheme. In turn they can enable all PV panels in a system to generate power despite unequal irradiation (Walker and Sernia, 2004). However, the shortcomings of this scheme are twofold. Firstly the operating point of each of these modules is constantly changing in response to a system disturbance even though it may be, for example, due to the variation in light intensity level experienced by the other modules in the chain (Kajihara and Harakawa, 2005). The other drawback is that the full power generated by each of these PV modules flows through their respective converters, causing additional power loss due to converters (Abdalla et al., 2012).

The differential power processing approach can alleviate these shortcomings, and has been researched over the last few years (Mao et al., 2018; Chen et al., 2019; Babu and Narasimharaju, 2020; Zhang et al., 2020; Alharbi et al., 2020). The two topologies for such systems are as shown in Fig. 1. They employ non-isolated DC-DC converters, such as those based on bidirectional buck-boost converter (Fig.1 (a)) or Ćuk converter circuits (Fig.1(b)) to form the PV-to-PV architecture. Note that these two converters are dual circuits. The Ćuk bidirectional converter uses capacitor C_n as energy storage whereas the buck-boost type uses an inductor. Both exhibit the same voltage transformation ratio for a given duty cycle k. The system using the buck-boost converter was modelled and successfully used (Schaef and Stauth, 2014), but the main problem of this converter is non-continuous input and output currents which potentially need large capacitors shunting the converter terminals or the PV modules. The other architecture uses an isolated converter, such as a flyback type, to link each of the serially connected PV generators to the common DC bus output, forming the PV-to-bus architecture. The key feature of these two forms is that under uniform solar irradiation, no PV generated power passes through the converters, and hence there is no converter power loss within them. When partial shading occurs only a fraction of the power generated by its associated PV modules, according to the differences between the irradiation levels, is processed by the converter. Though there is still conversion losses in the terminal DC-DC converters, or DC-AC inverters for grid connection, the total power throughput should be higher than for the continuous scheme. Two main requirements of the PV-to-PV

architecture (Bishop, 1988; Schaef and Stauth, 2014) make it more challenging to control. Firstly, a complete set of appropriate control schemes is needed to lead the system in achieving the maximum power point (MPP) operation. Secondly, the effect of the constantly changing PV operating points on the converter dynamics becomes the primary limiting factor for designing the system controller. In the authors' previous work, the first requirement was partly achieved by regulating the voltages of individual PV panels (Chong and Zhang, 2013), and then only by assuming that the PV voltage set points at the MPPs are already known.

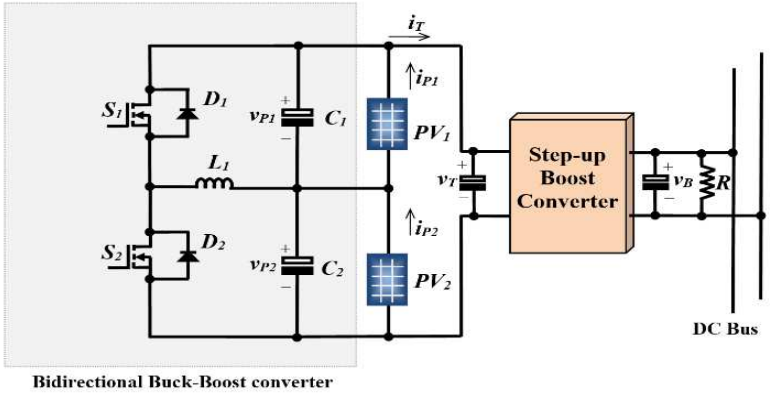

(a)

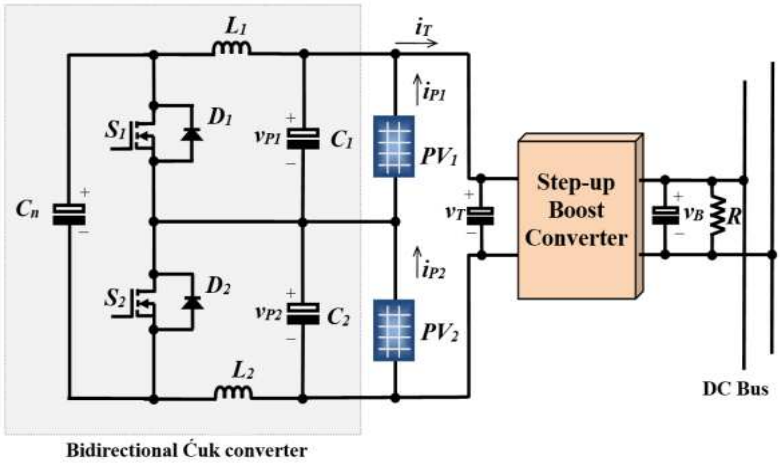

(b)

Fig. 1: Modules in differential PV power processing system: (a) bidirectional buck-boost converter and (b) bidirectional Ćuk converter

This paper presents a new MPPT controller using the proposed DWSSA algorithm for a PV generator formed by multiple bidirectional PVCC modules for PV panels under partial shading and module mismatching. The preference for the Ćuk converter over the buck-boost topology is due to the former having continuous current input and output currents, hence introducing smaller current ripple when charging and discharging the capacitors connected across the panel PV terminals. The configuration scheme with DWSSA-MPPT proposed for this PV power system estimates the individual MPP voltages of all the PV panels in the chain under a specific weather condition. With SSA estimated voltages a two-loop lead-lag control

scheme is then used to determine the switching state and duty ratio for both of the Ćuk converters connected to each PVCC in the chain. The parameters of the controller are tuned based on the transfer function model of the PVCC, which is also detailed in the paper.

The rest of the paper is organized as follows: Section 2 reviews the structure of the PVCC system. Section 3 presents in detail the DWSSA-based MPP tracking method. Derivation and experimental validation of a transfer function model of the PVCC are in Section 4. The model enables the setting of the PVCC controller parameters. Section 5 presents the principle and implementation of the control scheme for a general system having two or more PVCC modules. Section 6 presents the simulation of a PV system with two serially connected PVCCs and three PV panels, operating under variable irradiation and controlled by the proposed scheme.

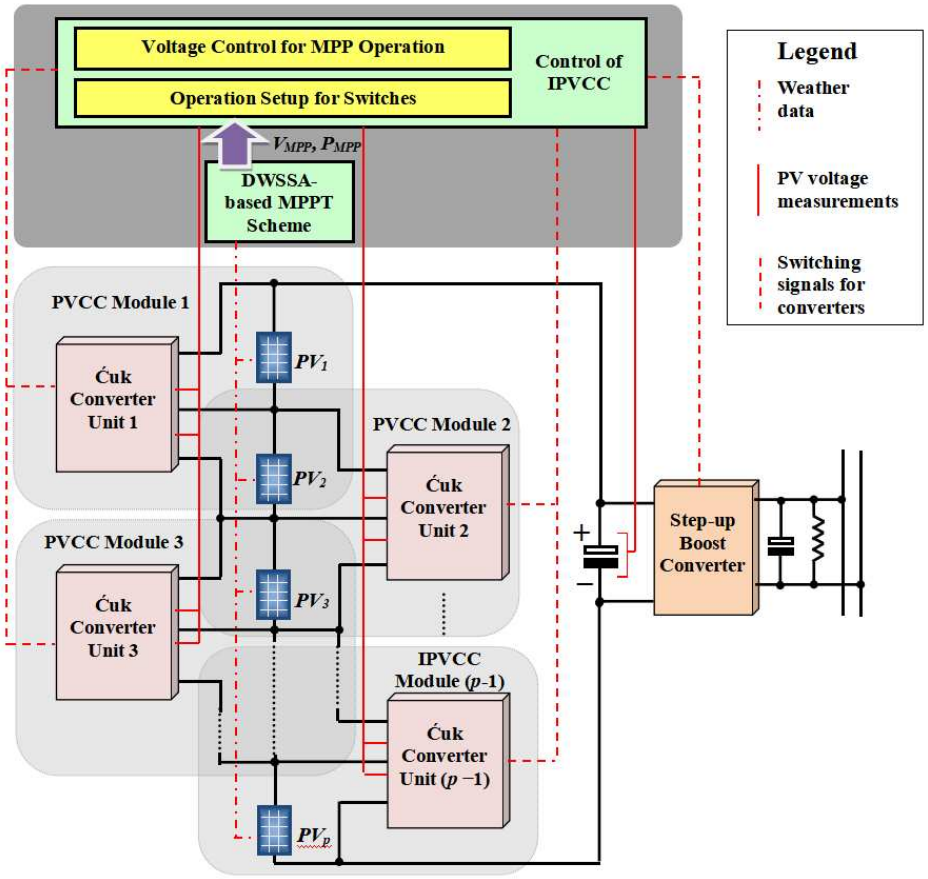

Fig. 2: Configuration of PV-Ćuk converter (PVCC) system

2. Configuration of the cascaded PVCC system

The system studied comprises multiple PVCC modules connected in series and a terminal step-up converter as shown in Fig.1(a). The circuit diagram of such a system with only a single PVCC module is shown in Fig.1(b). Each of the PVCC modules has a Ćuk bidirectional converter with its two terminal pairs connected to two serially linked PV panels (PV_1 and PV_2). Note that two adjacent PVCC modules are overlapped, namely they share one PV panel as shown in Fig.2. The advantage of using the Ćuk converter for two PV panels lies in its bidirectional feature, meaning that it can reverse the direction of both current and power

flow. This is necessary since the two PV panels at its terminal pairs may have either sense of differential irradiation so the input and output sides of the converter must be interchangeable.

The operating principle of this system was explained in detail in the authors' previous paper (Chong and Zhang, 2013). To summarise, the inner Ćuk converter is used to establish the ratio between the voltages of two chained PV panels. The terminal boost converter is used for regulating the summed voltage of two series connected PV modules to reach the total MPP voltage value. The key feature of this system lies in its two operating modes; one is when irradiation levels on two PV panels are the same. In this case the generated powers and currents from the PV panels are ideally the same, so the same current flows through the chained panels. Thus, with well-matched panels below some minimum threshold of illumination difference, the Ćuk converters which provide the current bypass path can be idled, giving infinitely high resistance along the path. For the second mode when the irradiations on the panels are different, i.e. the PV panels are partially shaded, their currents are different. The Ćuk converters are now required to provide a path for a portion of the PV current to flow. This can be done by regulating the two switch duty ratios of the Ćuk converter in the module, since it has the input and output voltage relationships given as (Chong and Zhang, 2013):

$$(A) \qquad \frac{V_{PV2}}{V_{PV1}} = \frac{k_1}{1-k_1}, \text{ when the light level on } \mathrm{PV}_1 \text{ is higher, and}$$

$$(B) \qquad \frac{V_{PV1}}{V_{PV2}} = \frac{k_2}{1-k_2}, \text{when } \mathrm{PV}_2 \text{ has the higher light level.}$$

where V_{PV1} and V_{PV2} are, respectively, the terminal voltages of PV panels 1 and 2, k_1 and k_2 are duty ratios for switches S_1 and S_2 as shown in Fig. 1 (b). Proper adjusting the switch duty ratio can ensure the terminal voltages of two solar panels are in the ratio of their MPP voltage values corresponding to their respective solar irradiation levels. Subsequently the terminal step-up converter ensures the sum of the PV panel voltages is at the MPP, hence achieving the global MPP (GMPP) tracking. The output of this converter may be connected to a DC-bus or a battery which must be controlled to the required voltage. Thus, the terminal capacitors of this converter are so chosen to eliminate the voltage ripples, hence it has a slower dynamic response speed compared to the inner Ćuk converters.

It is worth noting that the detection of partial shading relies on having light sensors fitted on all panels, these providing light intensity data which are processed periodically by the central controller. If light intensities for panels show significant differences, partial shading is identified.

The capabilities of this system as stated have been experimentally validated. The schematic of an experimental PVCC system is as shown in Fig. 3(a). This is comprised of two 100W PV modules and one Ćuk converter and a variable resistor is connected across its terminals to adjust the output voltage. The experiment was performed by setting different light levels on the two PV panels, and adjusting the converter switching duty ratio and the terminal resistance until each panel's output power reaches the maximum value corresponding to its irradiation level. The measurements of both voltage and power values for different

combinations of light conditions are shown in Table 1. Clearly, they match well with the actual MPP voltages and powers which were obtained through the measured individual P-V cures as shown in Fig. 3 (b). This experiment shows that the proposed architecture permits the two PV panels tracking their MPP voltages correctly as that given by their P-V characteristic curves. The global MPP voltage and power values of the unit are respectively the sums of the individual panel's values.

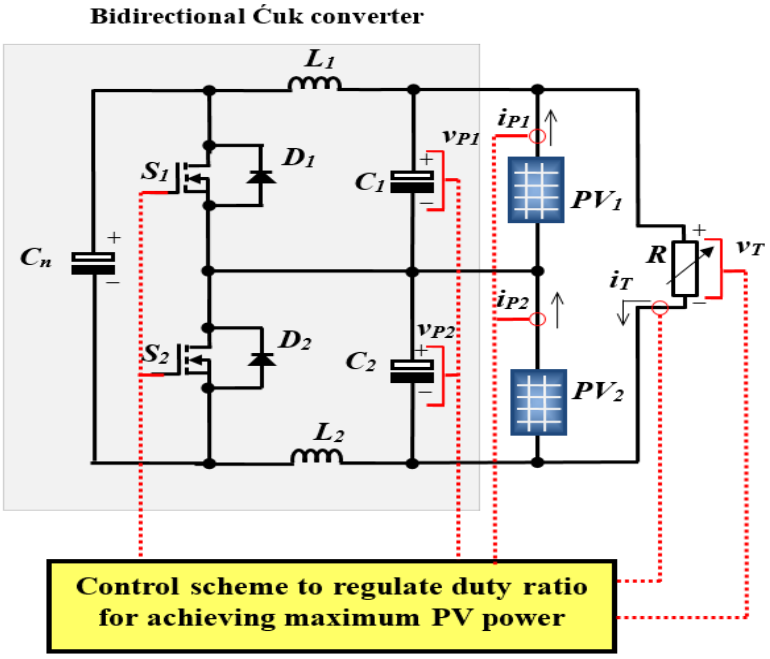

(a)

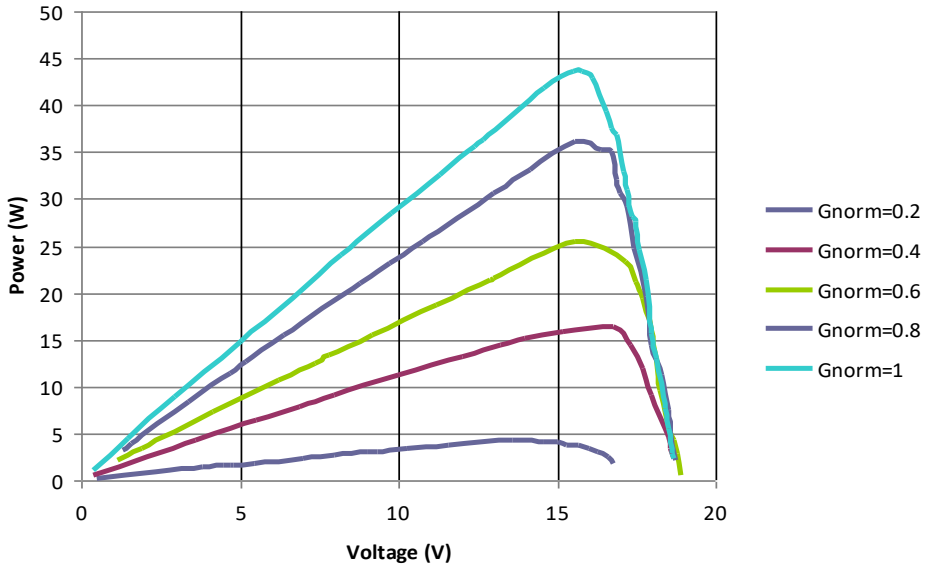

(b)

Fig. 3: (a) Schematic of Experimental test and (b) P-V curves of the PV panel used under different light levels.

Table 1 Results of an experimental PVCC unit with two PV panels tracking their respective MPPs under different irradiation levels

Weather conditions (in kW/m^2)		**Measured PV1 voltage (V)**	**Measured PV2 voltage (V)**	**Measured PV1 power (W)**	**Measured PV2 power (W)**	**Desirable MPP voltages (V)**		**Desirable MPP Power (W)**	
G_1	G_2					V_{MPP1}	V_{MPP2}	P_{MPP1}	P_{MPP2}
1.0	0.2	15.8	14.8	42.2	4.0	15.8	14.6	44.2	4.5
1.0	0.4	15.4	16.9	42.7	15.9	15.8	16.8	44.2	16.3
1.0	0.6	16.0	15.6	44.1	24.5	15.8	15.6	44.2	25.8
1.0	0.8	16.1	15.4	44.0	35.6	15.8	15.55	44.2	36.1

3. The proposed DWSSA-based MPPT Controller

To achieve the maximum power generation from this system, a control scheme is proposed as shown in the lower half of Fig. 1(a). This consists of two stages: the maximum power point voltage searching for all chain-linked PV panels corresponding to their measured light and temperature values, and the switching state determination and feedback control of Ćuk converters realizing the desired power generation.

3.1 The basic SSA description

SSA is proposed by Mirjalili et al. (2017). SSA has few control parameters, which can effectively avoid the problem that the optimization fails due to the unreasonable parameter setting. Specifically, the position of the basic SSA is updated (Mirjalili et al., 2017):

$$x_j^1 = \begin{cases} F_j + c_1((ub_j - lb_j)c_2 + lb_j), & c_3 \geq 0 \\ F_j - c_1((ub_j - lb_j)c_2 + lb_j), & c_3 < 0 \end{cases} \quad (1)$$

where j is number of dimensions, x^1_j and F_j represent respectively the first salp position and the food source position when the number of dimension is j. In addition, ub_j and lb_j is the upper and lower bound respectively when the number of dimension is j, and c_2, c_3 ~U(0, 1). The parameter c_1 is (Mirjalili et al., 2017):

$$c_1 = 2 \cdot e^{-(\frac{4l}{L})^2} \tag{2}$$

where L and *l* represent respectively the maximum iterations and the current iteration. The position update formula is (Mirjalili et al., 2017):

$$x_j^i = \frac{1}{2}at^2 + v_0 t \tag{3}$$

where v_0 is the initial speed. Considering $v_0 = 0$, the formula will be modified as (Mirjalili et al., 2017):

$$x_j^i = \frac{1}{2}\left(x_j^i + x_j^{i-1}\right) \tag{4}$$

3.2 The proposed DWSSA algorithm

In the course of iteration, the followers are influenced by each other. The interactions of followers influence the performance of the population, especially when the algorithm reaches its late iterative stage, the population converges the food source slowly. Therefore, in order to improve the speed and capability of exploitation, this paper proposes an improved SSA algorithm by introducing a dynamic *w* factor. Meanwhile, a random value ϕ which is within the interval (0, 1) is added to improve the search ability. Thus, the followers are updated as follows:

$$x_j^i = \frac{1}{2}\left(k * x_j^i + x_j^{i-1}\right) \tag{5}$$

$$k = \phi \cdot w, w = w_{max} - (w_{max} - w_{min}) * tan(\frac{1}{\varepsilon} * \frac{l}{L}\pi) \tag{6}$$

where ϕ is a random value within the interval (0,1), ε=4, w_{max} =0.9 and w_{min} = 0.2. In the initial stage of the iteration, the value of the proposed nonlinear convergence factor *w* decreases slowly as the number of iterations increases, which is conductive to intensify the exploration ability of the algorithm and find the global optimal solution. In the later stage of iteration, its value decreases rapidly in order to improve the speed and capability of exploitation. The graph of the value of the nonlinear convergence factor *w* with the number of iterations is shown in Fig. 4. Hence, the DWSSA has the better capability of balancing exploration and exploitation.

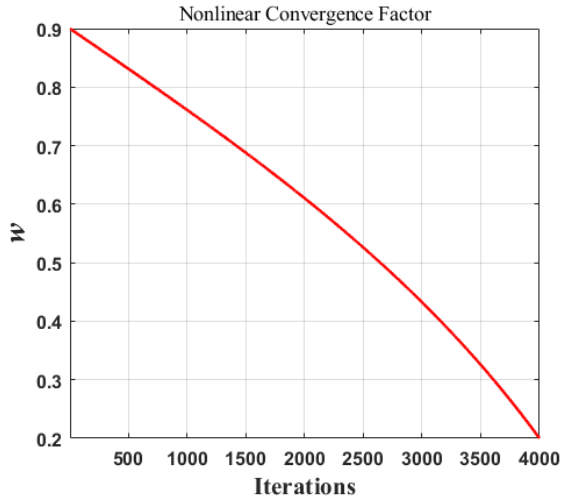

Fig. 4: The nonlinear convergence factor *w* with the number of iterations

3.3 DWSSA Based MPPT method

Applying the DWSSA to the system shown in Figure 1. Based on the references (Bishop, 1988; Mao et al., 2018), the fitness functions given as:

$$I_{out} = I_{sc} - I_o(exp\left[\frac{q(V_{out}+R_S I_{out})}{AKT_c}\right] - 1) - I_{shunt} \tag{7}$$

$$PVfitness(G,T,I_{out}) = I_{out} \times V_{out} \tag{8}$$

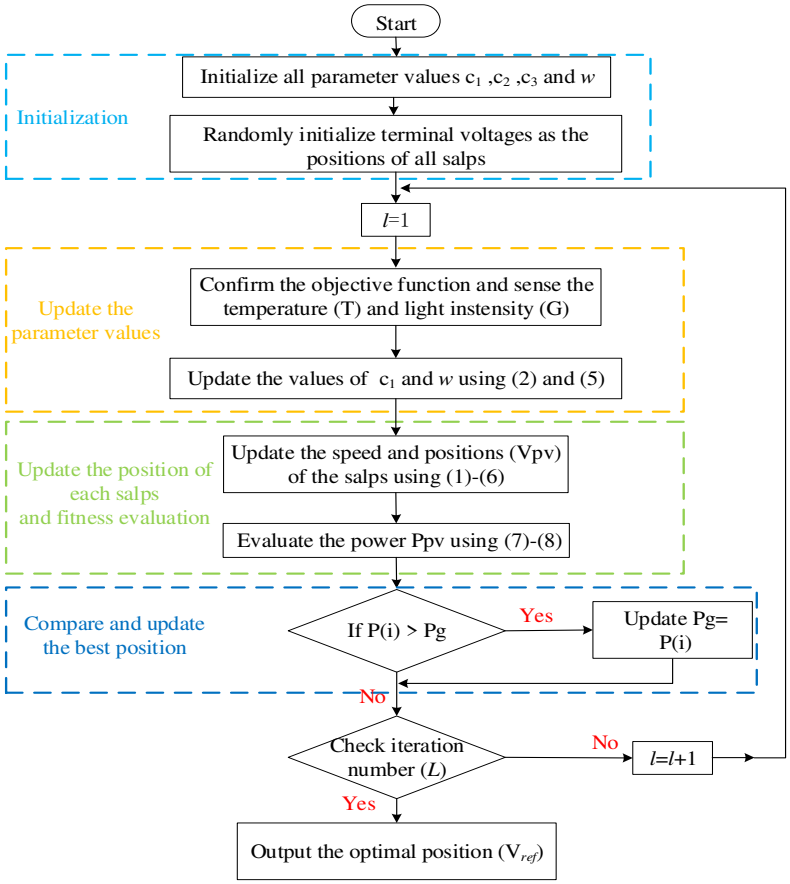

Fig. 5: Flowchart of the proposed DWSSA-MPPT method

The flowchart of the proposed DWSSA-MPPT method is shown in Fig. 5 and the procedures for implementing the DWSSA-MPPT controller are listed below:

i) Input the current temperature (T) and light intensity (G) and initialize the terminal voltages as positions of all salps using eqs. (1)-(6);

ii) Calculate the fitness values using eqs. (7)-(8) for each salp;

iii) Compare and update the position of the best salp in all of the salps;

iv) Check the specified number of iterations to exit the program and output the optimal position (V_{ref}), otherwise return to step ii).

4. Transfer Function Model of a PVCC Module

The estimated voltages from the SSA are then passed on to control the chained PVCC system. Each PVCC uses a lead-lag compensator whose parameters rely on accurate knowledge of the PV-Ćuk converter characteristics, thus a transfer function model for a PVCC module shown in Fig.3 needs to be derived. It is assumed that PV_1 receives higher solar irradiation than PV_2, hence S_1-D_2 is active. Since the PVCC module has left-right

symmetry this model is applicable to the alternative case. Continuous conduction is assumed. The method follows standard procedure of using a state variable vector **x** to describe the converter circuit in on and off states, and combining the resulting equations yields an average equation of the converter over one switching period. By introducing small ac perturbations of all variables in the average equation and taking their Laplace transform, the transfer functions expressed as the ratio between the changes of PV panel terminal voltage to duty ratio given as $\Delta v_{P1}(s)/\Delta k_1(s)$, or $\Delta v_{P2}(s)/\Delta k_2(s)$ are obtained, the detail is described in the following.

4.1 Transfer Function Model Derivation

For a PVCC module, the state vector $\boldsymbol{x} = [i_{L1} \quad i_{L2} \quad v_{P1} \quad v_{P2} \quad v_{cn}]^T$ consists of instantaneous voltages and currents of the converter. Two state vector equations for the converter at S_1 on and off states, are given in Appendix. Combining these two equations leads to a simplified overall average equation for one switching period, T_p, given as

$$\dot{\boldsymbol{x}} = \boldsymbol{A}_T\boldsymbol{x} + \boldsymbol{B}i_T + \boldsymbol{Q}_1 i_{P1} + \boldsymbol{Q}_2 i_{P2} \tag{9}$$

$$\boldsymbol{A}_T = \begin{bmatrix} 0 & 0 & \frac{1}{L_1} & 0 & -\frac{(1-k_1)}{L_1} \\ 0 & 0 & 0 & -\frac{1}{L_2} & \frac{k_1}{L_2} \\ -\frac{1}{C_1} & 0 & 0 & 0 & 0 \\ 0 & \frac{1}{C_2} & 0 & 0 & 0 \\ \frac{(1-k_1)}{C_n} & -\frac{k_1}{C_n} & 0 & 0 & 0 \end{bmatrix} \boldsymbol{B} = \begin{bmatrix} 0 \\ 0 \\ -1/C_1 \\ -1/C_2 \\ 0 \end{bmatrix}, \ \boldsymbol{Q}_1 = \begin{bmatrix} 0 \\ 0 \\ 1/C_1 \\ 0 \\ 0 \end{bmatrix} \text{and } \boldsymbol{Q}_2 = \begin{bmatrix} 0 \\ 0 \\ 0 \\ 1/C_2 \\ 0 \end{bmatrix}$$

where vectors **B**, Q_1 and Q_2 are parameters relating to the input variables of the model, and i_{P1}, i_{P2} and i_T are respectively the currents of the two PV panels and converter terminal currents.$k_1$is the duty cycle of S_1.

By introducing small ac perturbations in the dc steady-state quantities, and removing negligibly small elements, eq. (9) can be expressed as a small signal model given as

$$\Delta\dot{\boldsymbol{x}} = \boldsymbol{A}_{sm}\Delta\boldsymbol{x} + \boldsymbol{B}\Delta i_T + \boldsymbol{Q}_1\Delta i_{P1} + \boldsymbol{Q}_2\Delta i_{P2} + \boldsymbol{J}\Delta k \tag{10}$$

where$\Delta\mathbf{x} = [\Delta i_{L1} \quad \Delta i_{L2} \quad \Delta v_{P1} \quad \Delta v_{P2} \quad \Delta v_{cn}]^T$, $\mathbf{A}_{sm}$

$$= \begin{bmatrix} 0 & 0 & \frac{1}{L_1} & 0 & -\frac{(1-K_1)}{L_1} \\ 0 & 0 & 0 & -\frac{1}{L_2} & \frac{K_1}{L_2} \\ -\frac{1}{C_1} & 0 & 0 & 0 & 0 \\ 0 & \frac{1}{C_2} & 0 & 0 & 0 \\ \frac{(1-K_1)}{C_n} & -\frac{K_1}{C_n} & 0 & 0 & 0 \end{bmatrix} \text{and } \mathbf{J} = \begin{bmatrix} \frac{V_{P1}+V_{P2}}{L_1} \\ \frac{V_{P1}+V_{P2}}{L_2} \\ 0 \\ 0 \\ \frac{I_{P2}-I_{P1}}{C_n} \end{bmatrix}.$$

Δi_{P1} and Δi_{P2} are respectively current changes of PV_1 and PV_2, at one operating point under a specific weather condition and can be expressed as

$$\Delta i_{P1} = -\frac{\Delta v_{P1}}{R_{P1}} \text{ and } \Delta i_{P2} = -\frac{\Delta v_{P2}}{R_{P2}} \tag{11}$$

where $-\frac{1}{R_{P1}}$ and $-\frac{1}{R_{P2}}$ are the gradients of the PV panels' I-V curves at a specific point, and vary with the operating point. Substituting Δi_{P1} and Δi_{P2} in eq. (10) by eq. (11) leads to a simplified model as

$$\Delta \dot{\boldsymbol{x}} = \boldsymbol{A}^*_{sm}\Delta \boldsymbol{x} + \boldsymbol{B}\Delta i_T + \boldsymbol{J}\Delta k \tag{12}$$

where $\mathbf{A}^*_{sm} = \begin{bmatrix} 0 & 0 & \frac{1}{L_1} & 0 & -\frac{(1-K_1)}{L_1} \\ 0 & 0 & 0 & -\frac{1}{L_2} & \frac{K_1}{L_2} \\ -\frac{1}{C_1} & 0 & -\frac{1}{R_{P1}C_1} & 0 & 0 \\ 0 & \frac{1}{C_2} & 0 & -\frac{1}{R_{P2}C_2} & 0 \\ \frac{(1-K_1)}{C_n} & -\frac{K_1}{C_n} & 0 & 0 & 0 \end{bmatrix}$ and $\mathbf{J} = \begin{bmatrix} \frac{V_{P1}+V_{P2}}{L_1} \\ \frac{V_{P1}+V_{P2}}{L_2} \\ 0 \\ 0 \\ \frac{V_{P2}}{R_{P2}C_n} - \frac{V_{P1}}{R_{P1}C_n} \end{bmatrix}$.

The voltage perturbation across PV_1 is then given as

$$\Delta v_{P1} = [0 \quad 0 \quad 1 \quad 0 \quad 0]\boldsymbol{\Delta x} = \boldsymbol{Z_1 \Delta x} \tag{13}$$

Likewise $\Delta v_{P2} = [0 \quad 0 \quad 0 \quad 1 \quad 0]\boldsymbol{\Delta x} = \boldsymbol{Z_2 \Delta x}$

The bidirectional Ćuk converter is designed assuming any of the two PV panels can be shaded, and the same power level will flow in both directions through the converter. Therefore for the same steady state voltage and current ripple requirements, the converter's passive components are chosen such that $L_1 = L_2$ and $C_1 = C_2$.

The outer boost converter shown in Figure 1 is used to deliver the total system generated power to the load and/or to a DC-bus. The power rating of the boost converter is high, at least, equal to the sum of all chained PV panels and has a much slower dynamics than any of the PVCC module. This implies that the terminal current ripple, Δi_T, which is controlled by this converter can be assumed to be near zero, and the terminal voltage remains constant, i.e. $V_T = V_{P1} + V_{P2} + \ldots + V_{Pn}$. Thus term $\boldsymbol{B}\Delta i_T$ in eq.(12) is eliminated.

Taking the duty ratio Δk_1 as the control variable and the voltage across PV_1 as the controlled variable, the transfer function between them is written as

$$G_{v1}(s) = \frac{\Delta v_{P1}(s)}{\Delta k_1(s)} = \boldsymbol{Z_1}(s\boldsymbol{I} - \boldsymbol{A}^*_{sm})\boldsymbol{J} = -\frac{\beta_3 s^3 + \beta_2 s^2 + \beta_1 s + \beta_0}{\alpha_5 s^5 + \alpha_4 s^4 + \alpha_3 s^3 + \alpha_2 s^2 + \alpha_1 s + \alpha_0} V_T \tag{14}$$

where the numerator coefficients are given by

$$\beta_3 = CC_nL,\ \ \beta_2 = \frac{C_nL}{R_{P2}} + CL(1-K_1)\left(\frac{(1-K_1)}{R_{P1}} - \frac{K_1}{R_{P2}}\right),$$

$$\beta_1 = C_n + CK_1 + \frac{L(1-K_1)}{R_{P2}}\left(\frac{(1-K_1)}{R_{P1}} - \frac{K_1}{R_{P2}}\right) \text{ and } \beta_0 = \frac{(1-K_1)^2}{R_{P1}} + \frac{{K_1}^2}{R_{P2}} \quad (15)$$

and those for the denominator can be written as

$$\alpha_5 = (CL)^2C_n,\ \alpha_4 = CC_nL^2\left(\frac{1}{R_{P1}} + \frac{1}{R_{P2}}\right),\ \alpha_3$$
$$= C_nL\left(2C + \frac{L}{R_{P1}R_{P2}}\right) + C^2L\left({K_1}^2 + (1-K_1)^2\right),$$
$$\alpha_2 = L\left(C_n + C{K_1}^2 + C(1-K_1)^2\right)\left(\frac{1}{R_{P1}} + \frac{1}{R_{P2}}\right),$$
$$\alpha_1 = C_n + \left({K_1}^2 + (1-K_1)^2\right)\left(C + \frac{L}{R_{P1}R_{P2}}\right) \text{ and } \alpha_0 = \frac{(1-K_1)^2}{R_{P1}} + \frac{{K_1}^2}{R_{P2}} \quad (16)$$

Note in above equations $C = C_1 = C_2$, $L = L_1 = L_2$. Transfer function for the voltage across PV_2 and the duty ratio k_2, i.e. $G_{v2}(s) = \frac{\Delta v_{P2}(s)}{\Delta k_2(s)}$ is similar to eq. (14) with the same denominator but the coefficients for the numerator become

$$\beta_3 = CC_nL,\ \beta_2 = \frac{C_nL}{R_{P1}} + CLK_1\left(\frac{K_1}{R_{P2}} - \frac{(1-K_1)}{R_{P1}}\right),$$

$$\beta_1 = C_n + C(1-K_1) + \frac{LK_1}{R_{P1}}\left(\frac{K_1}{R_{P2}} - \frac{(1-K_1)}{R_{P1}}\right), \text{ and } \beta_0 = \frac{(1-K_1)^2}{R_{P1}} + \frac{{K_1}^2}{R_{P2}} \quad (17)$$

According to the denominator of eq. (14), all poles are on the left-hand-side s-plane, hence both G_{v1} and G_{v2} are stable 5th order systems, but the numerators may have right-hand-side *s*-plane zeros as either β_1 or β_2 may become negative when $\frac{(1-K_1)}{R_{P1}} > \frac{K_1}{R_{P2}}$in eqs.(15) and (17). Since these two parameters are also functions of C_n and C_nxL,, these component values are selected to ensure that both β_1 and β_2 are greater than zero under all possible operating conditions of K_1, R_{P1} and R_{P2}.

Note that the above model represents only one PVCC module. When the system has two or more such modules, multiple of this model can be used and each is for its corresponding module. The control can be performed on each module treating the variations from adjacent modules as interferences. Fast and non-oscillatory responses for individual PVCC voltage and current can be obtained provided the controller is well designed and parameters are adequately tuned. The controller tuning is based on the model derived above and this will be presented in sub-section 5.2.

4.2 Experimental Validation and Analysis of the Dynamical Model for the IPVCC

The above transfer function model has been validated using an experimental set-up having two identical PV panels (Sunsei SE-6000) connected on two terminals of a bidirectional Ćuk converter. The photographs of PV panels with the converter under two

identical in-house built controllable sun light simulators are given in Fig. 6(a)-(c).The light level for each sun-simulator can be varied from zero to its maximum value (i.e., 0 to 100%) which corresponds to a solar irradiation of 0.505 kW/m^2. The parameters of the converters in the experimental set-up are given in Table 2. Note that Inductors L_1 and L_2 are filters only to eliminate the inrush current when switching on or off either S_1 or S_2 to charge and discharge capacitor C_n. The inrush current frequency is very high hence inductor values need to be small. Too high inductor value leads to slow converter response speed to the changes of duty ratio. The main energy storage component C_n is set to 82 *uF*, a lot higher than the capacitors C_1 and C_2 across two PV modules. A microcontroller of dsPIC30F4011 is used to generate the PWM signals for the switches. Based on the schematic circuit in Fig. 2, the outer Boost converter connected at the bidirectional Ćuk converter terminals keeps terminal voltage V_T at 30.7 V. This is achieved by connecting a 60V DC supply at the boost converter load terminals with a load resistor of 35 Ω.

Table 2 Experimental circuit parameters

Ćuk Converter $L_1 = L_2$	2.2mH
Ćuk Converter $C_1 = C_2$	22μF
Ćuk Converter C_n	82μF
Terminal Capacitor C_T	470μF
Switching Devices	MOSFETs: STB24NF1 Diodes: DPG10I300PA
Switching Frequency	20kHz
Load Resistance	35.Ω

The experiments were performed by setting the irradiation levels of the two solar simulators to give 100% for PV_1 and 40% for PV_2. The corresponding I-V curves measured from these two panels are shown in Fig. 6(d).

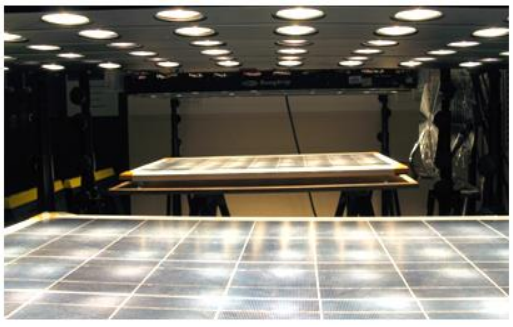

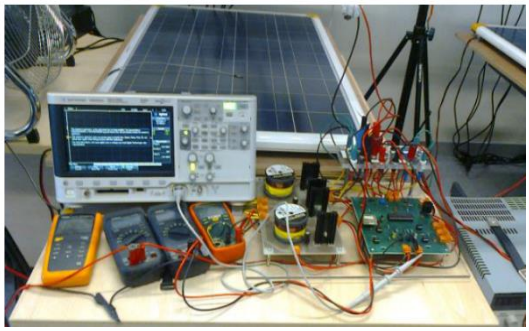

(a) (b)

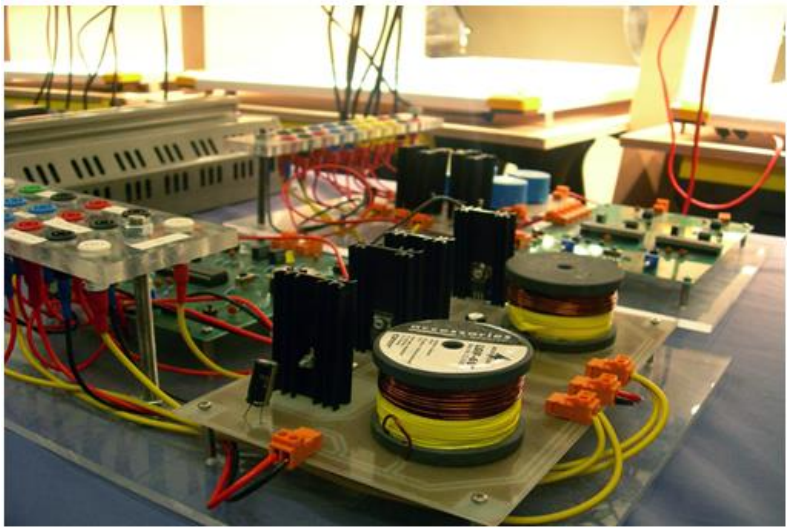

(c)

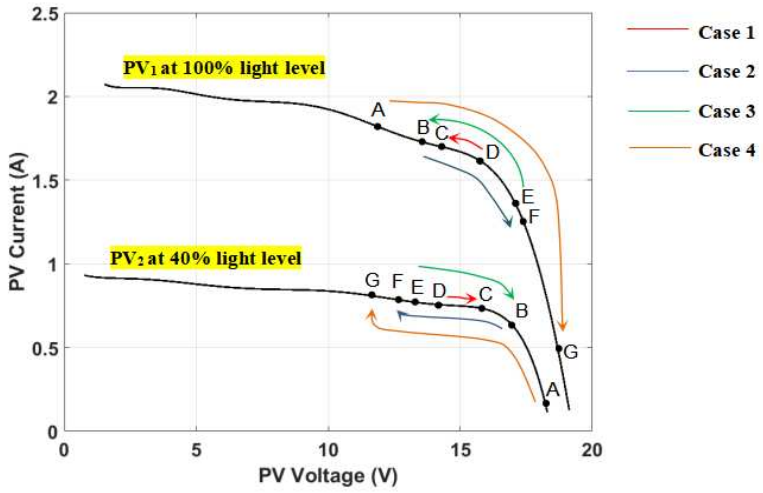

(d)

Fig.6: Experimental setup: (a) PV panels and solar simulator system, (b) Ćuk converter circuit for one PVCC module, (c) Multiple Ćuk converter modules circuit and (d) I-V characteristics for the PV panel under different light levels.

In this condition, since PV_1 was irradiated with higher light level than that of PV_2, the S_1-D_2 device pair was activated. Four different step responses of PV_1 and PV_2 voltage were performed so that the voltage was varying from one operating point to another as notated on both I-V curves in Fig. 6(d), including the four cases when the seven operating points (A, B, C, D, E, F and G) changes from D to C (Case 1), from B to F (Case 2), from E to B (Case 3), and from A to G (Case 4). They also correspond to a step change in K_1, from 0.46 to 0.52 for Case 1, from 0.43 to 0.58 for Case 2, from 0.57 to 0.43 for Case 3, and from 0.40 to 0.59 for

Case 4. All these cases cover a voltage range of 12-18 V corresponding to the MPP voltages under a wide range of weather conditions. The four step responses were measured using KEYSIGHT DSO-X-2014A 100 MHz Oscilloscope and are presented in Fig. 7(a). These are in close agreement with the responses in Fig. 7(b) which have been simulated in MATLAB using the transfer function derived in Section 3. The system poles and zeros for all the cases are shown shown in Fig. 7(c) and their positions vary from one case to another as R_{P1} and R_{P2} are changing with the voltage and weather conditions. Nevertheless for all the cases, the effects of the complex pole pairs nearer to the imaginary axis are cancelled by the adjacent zeros. The performance factors for all the four cases and the explanation on how they are related to the pole-zero diagram are summarized below:

Case 1: v_{P1} experiences a decrease from 16 to 14V. It has an under-damped step response with an overshoot of 40% which is relatively high. This can be explained by the dominant effect of the imaginary poles which are not cancelled by the system zeros. Therefore, the step response takes more than 5 ms to settle down to another steady state.

Case 2: v_{P1} increases from 13.3 to 17.8V. Because all the imaginary poles have been cancelled by the system zeros, v_{P1} has an over-damped step response and the settling time is about 4 ms.

Case 3: v_{P1} decreases from 17.5 to 13.3V and the transient response is similar to Case 1 because the imaginary poles have not been totally cancelled. Nevetheless, there is more damping effect in its response lowering the amount of overshoot and reducing the settling time to about 4 ms.

Case 4: v_{P1} experiences the greatest voltage change from 12.2 to 18.3 V. The cancellation of imaginary pole-zero has not been completely achieved. Therefore, higher order dynamics become more dominant leading to the high frequency oscillation at the onset of the step response.

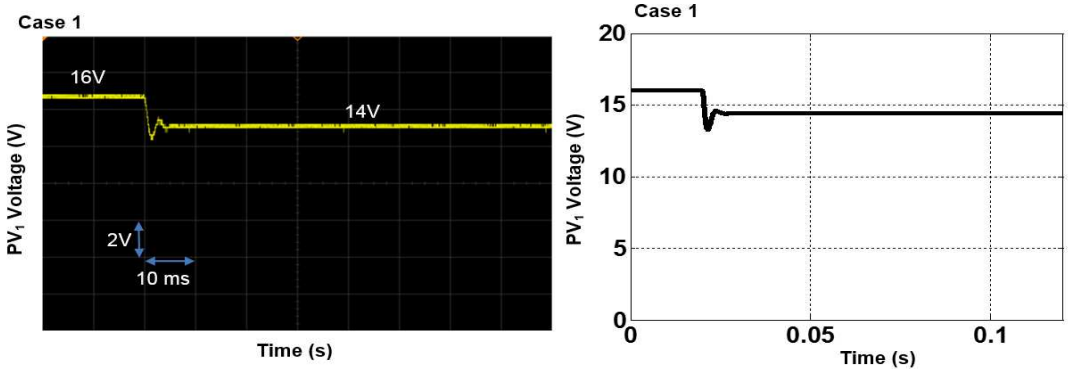

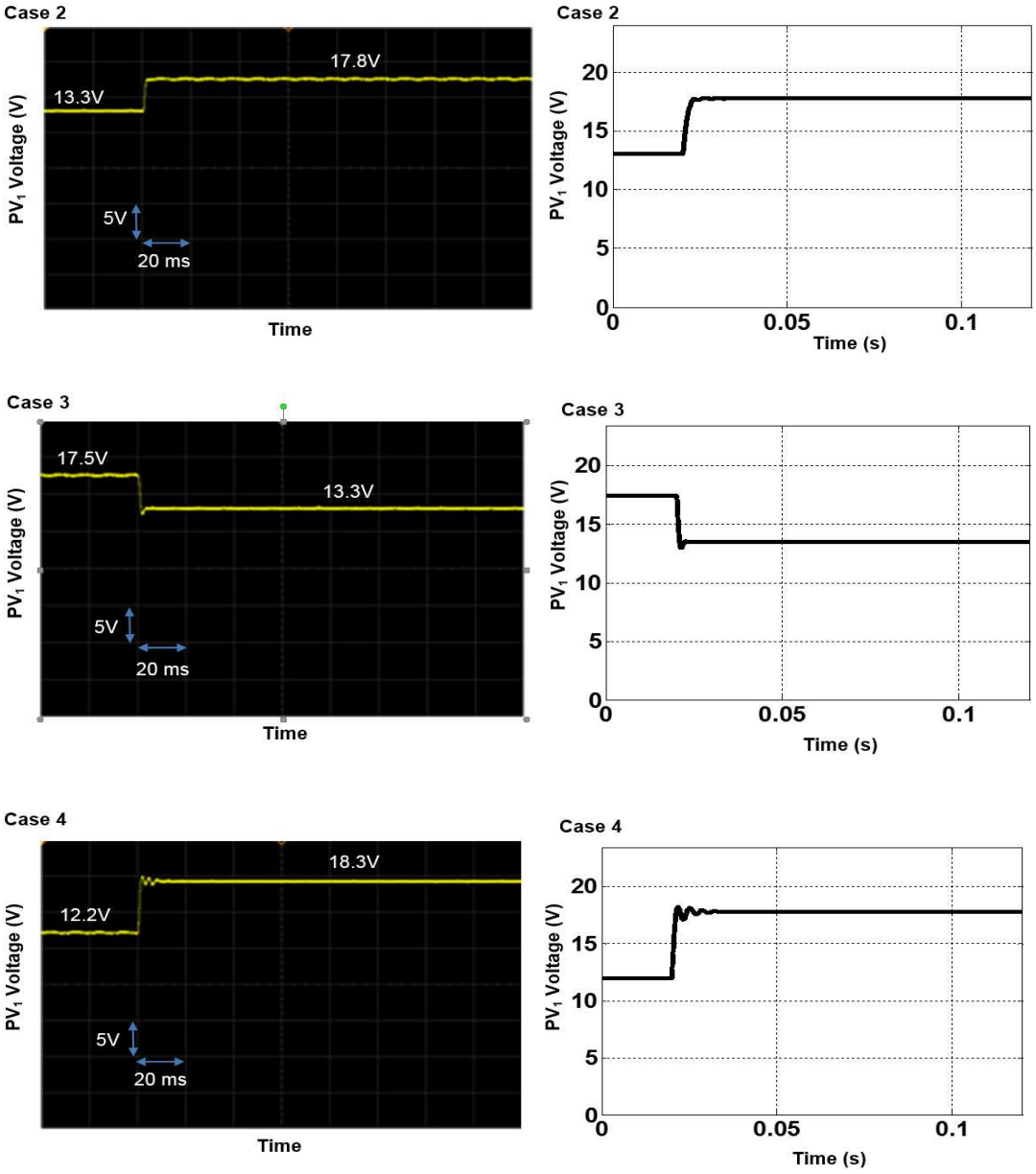
Case 2
17.8V
13.3V
5V
20 ms
Time
PV1 Voltage (V)
Case 2
PV1 Voltage (V)
Time (s)
Case 3
17.5V
13.3V
5V
20 ms
Time
PV1 Voltage (V)
Case 3
PV1 Voltage (V)
Time (s)
Case 4
18.3V
12.2V
5V
20 ms
Time
PV1 Voltage (V)
Case 4
PV1 Voltage (V)
Time (s)

(a) (b)

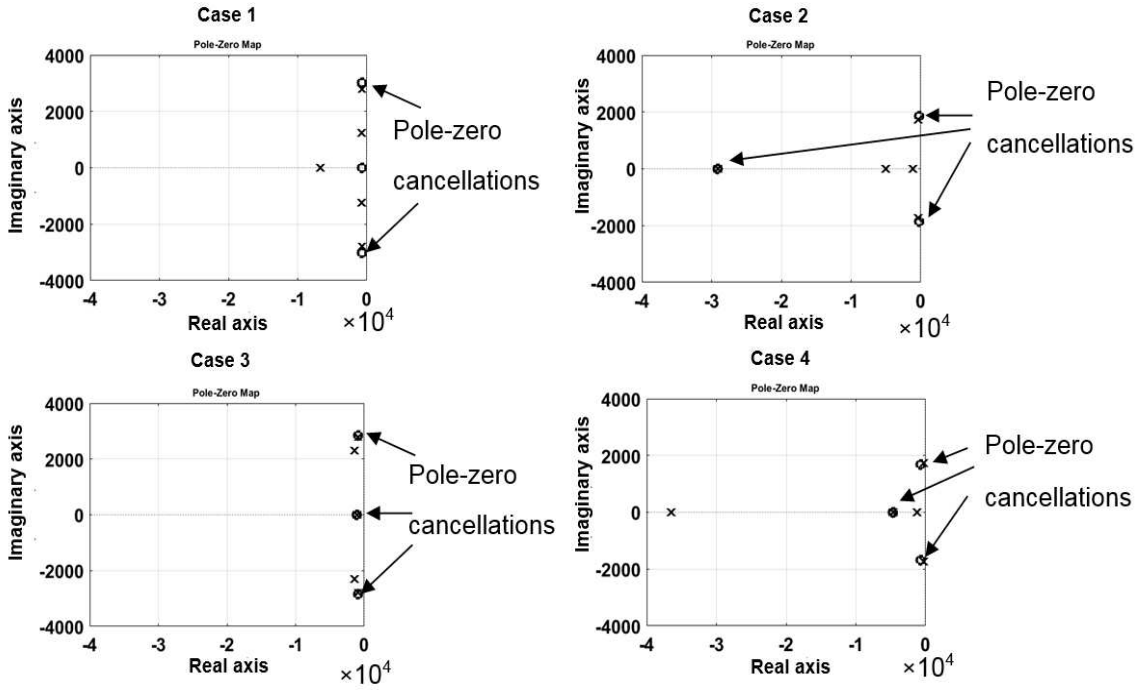

(c)

Fig. 7: Dynamical model verification for PVCC: (a) Experimental step responses, (b) Simulated step responses and (c) pole-zero diagram for Cases 1, 2, 3 and 4.

5. Model-Based Control of a Chained PVCC System

The above validated model is then applied to tune the parameters of the voltage lead-lag compensators for controlling the chained PVCC as shown in Fig.2 in order that all PV panels in the chain can track their SSA evaluated MPP voltages. The requirement for the controller is that the tracking to be fast and accurate with the minimum fluctuation when a sudden change of weather condition occurs. With multiple PVCCs in a chain, all PV panels should be controlled to operate at their respective MPPs, thus coordinated control is required for both the inner bidirectional Ćuk and terminal Boost converters.

5.1 Active Switch Pair Selection

When there is only one PVCC as shown in Fig. 1(b), the device pair that is required to be active can be determined by comparing the solar irradiations as described in the authors' previous work in (Chong and Zhang, 2013). Thus, one can vary S_1-D_2 duty cycle to control PV_2 voltage, treating PV_1 as constant, or S_2-D_1 to control PV_1 voltage treating PV_2 as constant according to voltage and current relationships given in (1).

In the case when SSA is used, the switching pairs are chosen according to SSA predicted power. If SSA estimated maximum power from PV_1 is greater than that of PV_2 i.e.. $P_{max1} > P_{max2}$ and the currents at the MPPs are $i_{L1} > i_{L2}$, S_1-D_2 pair is set active and the current bypass

path is through L_1. Otherwise when $P_{max1} < P_{max2}$ and $i_{L1} < i_{L2}$, S_2-D_1 is set active hence L_2 becomes current bypass path.

In a system having two or more PVCC modules in a chain, the selection of switch pair being active in one PVCC becomes more complex. Fig. 8 shows a system with *p* PV panels and *p-1* PVCC modules, setting the switch pair being active in each PVCC can be done by checking the current flowing through the node connecting two adjacent PV panels. For example the currents flowing in and out of the j^{th} node in this system are the current difference between j^{th} and $(j\text{-}1)^{th}$ PV panels and/or the current from the *j*, *(j-1)* and $(j\text{-}2)^{th}$ PVCC modules. Therefore the current flowing through L_1 in j^{th} converter can be written as

$$I_{L1j} = \left(I_{Pj} - I_{P(j-1)}\right) + \left(I_{L1(j-1)} + I_{L2(j-1)}\right) - \left(I_{L2(j-2)}\right), \tag{18}$$

and according to current relationship given in eqs.1(A) and (B), the current through L_2 of the same converter is

$$I_{L2j} = I_{L1j}\left(\frac{K_{2j}}{1-K_{2j}}\right) = I_{L1j}\left(\frac{1-K_{1j}}{K_{1j}}\right) = I_{L1j}M_j \tag{19}$$

where K_{1j} and K_{2j} are the respective duty ratios for S_1 and S_2 of j^{th} PVCC unit. Using eq. (19) to substitute all I_{L2j} terms in eq. (18) leads to

$$I_{L1j} = \left(I_{Pj} - I_{P(j-1)}\right) + \left(I_{L1(j-1)}\left[1 + M_{(j-1)}\right]\right) - \left(I_{L1(j-2)}M_{(j-2)}\right) \tag{20}$$

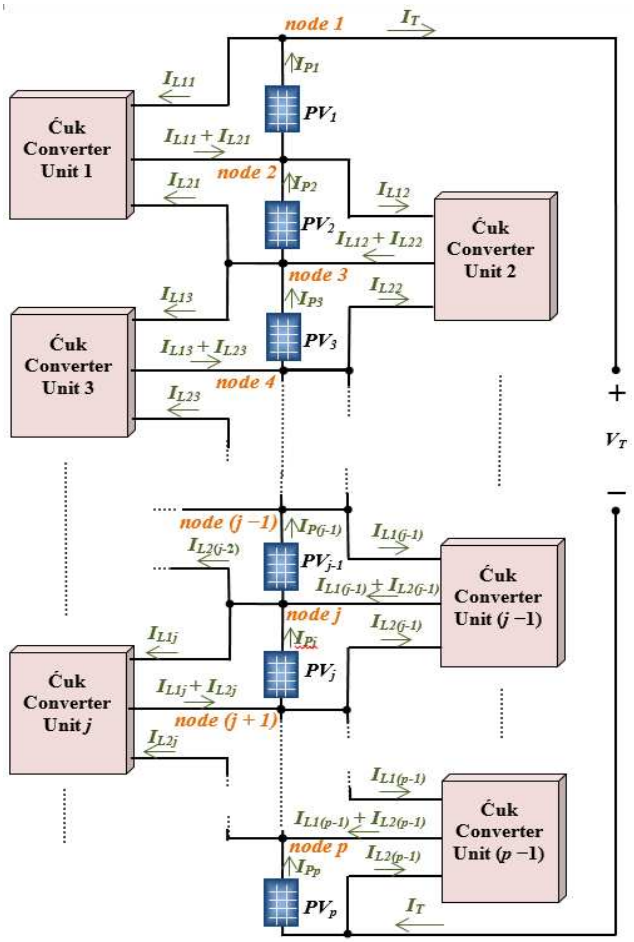

Fig. 8: Structure of a PVCC system with p modules

This can be used to determine the active switch pair in each PVCC module as follows:

1) Obtain the P_{MPPn} (n=1, 2, …) and corresponding V_{MPPn} for all PV panels in the chain from the SSA-based maximum power tracking scheme described in Section 3.

2) Estimate all the PV currents I_{Pn} using the obtained P_{MPPn} and V_{MPPn} and the desirable M_j terms (i.e., M_1, M_2, …, M_j, …, $M_{(p-1)}$). Note that M_j is the ratio between the j^{th} and $(j+1)^{th}$ PV panels respective maximum power voltages.

3) Evaluate the first PVCC converter current as $I_{L11} = I_{P1} - I_T$ where terminal current is

$$I_T = \frac{\sum_{j=1}^{p} P_{MPPj}}{\sum_{j=1}^{p} V_{MPPj}} \tag{21}$$

4) Iteratively evaluate I_{L1j} using eq. (20) for j = 2, 3, ….,p-1.

5) If $I_{L1j} > 0$, S_1-D_2 device pair in the j^{th} PVCC module is activated, otherwise S_2– D_1 pair in this module is activated.

5.2 Voltage Feedback control of Ćuk Converters

Once the active switch pair in the Ćuk Converter of each PVCC is chosen, a two-loop control scheme is applied, instead of using a two-input-two-output control scheme. This is because that each PVCC, once its switching pair is determined, is a uni-directional converter, i.e. one PV voltage connected to the converter can be assumed the input source and maintained constant, the other is the controllable output. Though the input end voltage may vary due to the changes of adjacent unit, such variations can be considered disturbances and can be eliminated. Following the two-loop control, the duty ratio the converter is firstly determined according to the two PV voltages to follow the SSA predicted maximum power values. As shown in Fig. 9, there is a main loop and a detuning loop $H_i(s)$ (i=1,2) for j^{th} PVCC, if the active switch pair is S_2-D_1 for the jth PVCC unit, so j^{th} PV panel voltage is controlled in the main loop, while the $(j+1)^{th}$ PV voltage is maintained by detuning the control signal from the main loop. The controllers are lead-lag compensators, and their parameters are tuned according to the transfer function model derived in Section 4. Parameter tunings of the lead-lag compensators follow the observations of model in sub-sections 4.1.and involves two major steps:

a) According to the compensator transfer function given as

$$H_i(s) = -N_i \left(\frac{\alpha_i \tau_i s+1}{\tau_i s+1}\right)\left(\frac{s+\beta_i}{s}\right) \tag{22}$$

where the parameters N_i, α_i, τ_i and β_i can be chosen assuming a given set of weather condition and the model of eq.(11) is identified. The requirements to the closed loop system are having a phase margin of 60^o and an overshoot of no more than 10% for a step response.

b) At a different operating point due to duty ratio change and under different weather conditions, the compensators designed in step 1 may need returning. This may be done by applying a step response on the model which is embedded in the control software. The model response enables identifying the rise time, t_r, and settling time, t_o and hence the system damping ratio, ζ, based on the design formula given in [28]. Adjusting compensator parameters can lead to desired damping ratio.

Note a P+I feedback control scheme is employed to adjust the duty ratio of the terminal boost converter. This controller takes boost converter output voltage as the constant since it may be connected to a battery or a dc-bus and regulates the input voltage to the level determined by the sum of the individual PV panel's MPP voltages. The P+I controller parameters are tuned by trial and error. The inner lead-lag compensator has a higher transient speed, and operates multiple samples per outer loop sample period. Until it completes its fixed samples the outer terminal voltage control loop can be activated. A complete flowchart summarizing the individual components of the MPP control scheme is shown in Fig. 10.

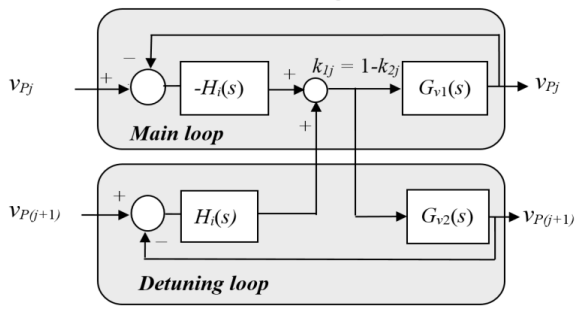

Fig. 9: Two loop control scheme for controlling the PV array terminal voltages

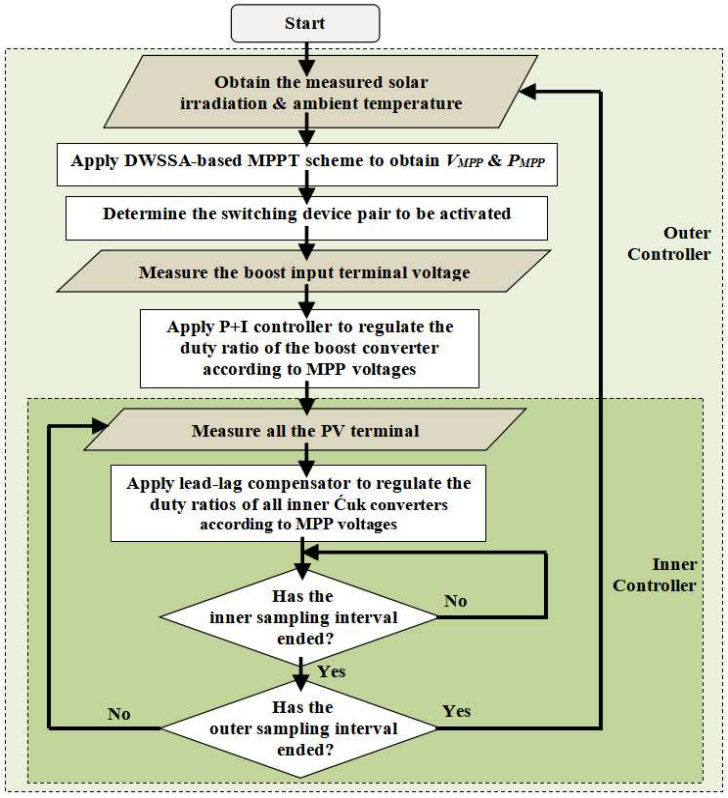

Fig. 10: Flowchart for the overall MPPT control scheme

6. Simulation Results & Discussions

The DWSSA-MPPT controller proposed above was applied to a computer simulation of a PV system consisting of two PVCC modules as shown in Fig. 1(b) and the performance of the overall system is verified. Moreover, the proposed scheme with DWSSA method is evaluated comprehensively by comparison with using the existing SSAPSO, SSAGWO, SSA and GWO methods under partial shading and mismatching. Table 3 lists the main parameters of DWSSA, SSAPSO (Ali et al., 2018), SSAGWO (Wan et al., 2019), SSA (Mirjalili et al., 2017) and GWO (Mohanty et al., 2016). The maximum iteration of DWSSA, SSAPSO, SSAGWO, SSA and GWO is set to 20, and the number of these algorithms is set to 10. This has three nominally identical PV panels (i.e., PV_1, PV_2 and PV_3); PVCC module 1

(PVCC1) is connected between PV_1 and PV_2 while PVCC module 2 (PVCC2) between PV_2 and PV_3. The system is implemented in MATLAB-SIMULINK software platform. The parameters of the PV system are listed in Table 4. Note that the L_B is the essential energy storage element for the terminal step-up converter. Its value is chosen according to voltage applied cross the inductor, switching frequency and also the desired current ripple $\Delta I/I_L$ which is set about 5%. The standard formulae for L_B value is $L_B = \frac{\Delta I \times k \times T_S}{V_{in}}$. In this application with the switching frequency of 5 kHz and input voltage per panel 20 V, k being 0.5, 12 mH is already a much larger value than calculated but a good compromise between obtaining a lower ripple current and faster converter response speed. Fig. 11(a)-(b) show the current-voltage and power-voltage curves of the PV panel under different irradiance levels. The three PV panels in the system are tested under three different light irradiation conditions as shown in Fig. 12 and the voltage responses of the individual PV panels are shown in Fig. 13(a)-(d). Detail explanations are summarized below:

a) From $t = 0$ to $t = 0.2$ s, PV_2 always receives the least solar irradiation while PV_1 and PV_3 are equally irradiated. The MPP tracking scheme in Section 3 estimates the maximum PV powers of each panel and their corresponding voltages while according to switch pair setup in Section 5.1 S_1-D_2 of PVCC1 and S_2 –D_1 of PVCC2 should be activated. This prompt both lead-lag compensators for the inner Ćuks and the P+I controller of the terminal boost converter to regulate the duty ratios until the MPP voltages are reached. Following a step change in G_2 around $t = 0.1$ s, the voltage in PV_2 takes 0.03 s to reach the new MPP operating voltage. the voltages across $PV_1$and PV_3 are disturbed and take about 0.04 s to recover to their original states.

b) From $t = 0.2$ to $t = 0.5$ s, all PV panels receive different solar irradiation throughout the period. At $t = 0.2$ s active switch pair for PVCC1 is still S_1-D_2but for PVCC2 its S_1-D_2 becomes active since $G_2 > G_3$. Both V_{PV2} and V_{PV3} are controlled to their MPP values while $V_{PV1}$is maintained to its original value for MPP generation after a small disturbance. At $t =$ 0.3 s, G_1 reduces to below G_2, while G_2 and G_3 are unchanged. V_{PV1} is regulated to the value estimated by SSA algorithm as expected, but both V_{PV2} and V_{PV3} are maintained to their respective MPP values despite small disturbances. Similarly, when G_3 has a step increase at $t = 0.4$ s, active switch pair in PVCC2 becomes S_1-D_2, while that in PVCC1 is unchanged. As shown in the Fig. 13(c) V_{PV3} is controlled to its desired level in about 0.05 S but V_{PV1} andV_{PV2} maintain their original values even though they are disturbed due to operation point changes. Fig. 13(d) shows variations of corresponding terminal voltage V_T. As can be seen, V_T is always equal to the sum of all three PV panels' MPP voltages under all light intensities.

The total power delivered to the load, including sum of maximum power values found from the three PV sources (Ppv), DWSSA, SSAPSO, SSAGWO, SSA and GWO methods are shown in Fig. 14. In addition, Table 5 shows some numerical values of simulated total power delivered to the load by 5 methods under the five cases respectively. It can be observed from Fig. 14 and Table 5 that the power generated by each PV module is changing with the weather conditions. An amount of time is required to execute the DWSSA-MPPT method and therefore, MPP operation may not be fully achieved when the solar irradiation is still changing. When they have stopped changing (or their variation becomes minimal), the overall system can then be controlled to deliver all the MPP power from each PV panel to the load. There is a small discrepancy between the extracted PV power and that estimated by the MPPT algorithm. This is due to the losses (within 2W) in the switches and diodes which are modelled as non-ideal devices in MATLAB-SIMULINK. In addition, the proposed DWSSA method outperforms the existing SSAPSO, SSAGWO, SSA and GWO methods in terms of convergence speed and accuracy in most cases, especially, in the most severe partial shading and module mismatching (From $t = 0.3$ to $t = 0.4$ s).

Table 3 The main parameters for the two algorithms

Algorithm	Parameter settings
DWSSA	a and ω: Self-adaption
SSAPSO	w and C_{1SSA}: Self-adaption, $C_{1PSO} = C_{2\,PSO} = 2$
SSAGWO	a and C_1: Self-adaption
SSA	C_1: Self-adaption
GWO	a: Self-adaption

Table 4 System parameters used in simulations

Symbol	Parameter	Value
V_{oc}	Open circuit voltage (at $G = 1$ kW/m^2 and $T = 20^oC$)	20V
I_{sc}	Short circuit current (at $G = 1$ kW/m^2 and $T = 20^oC$)	3.3A

L_1 & L_2	Inductors for PVCC1 and PVCC2	8 mH
C_n	Inner capacitor for PVCC1 and PVCC2	10 μF
C_1, C_2 &C_3	Terminal capacitor for a PV panel	20μF
L_B	Inductor for boost converter	12 mH

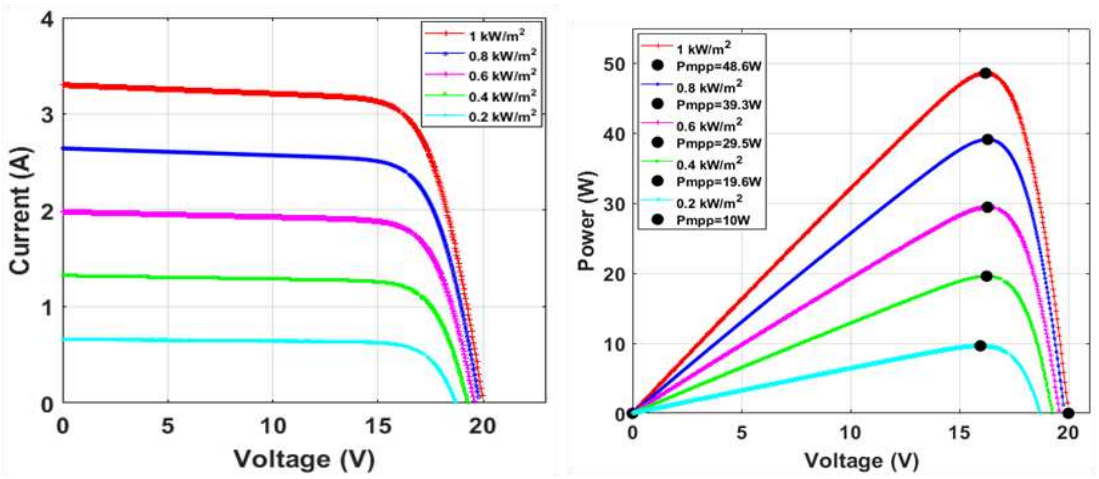

(a) (b)

Fig. 11: Electrical characteristics of the PV panel: (a) the I-V curves and (b) P-V curves under different irradiation for constant temperature of T=20℃

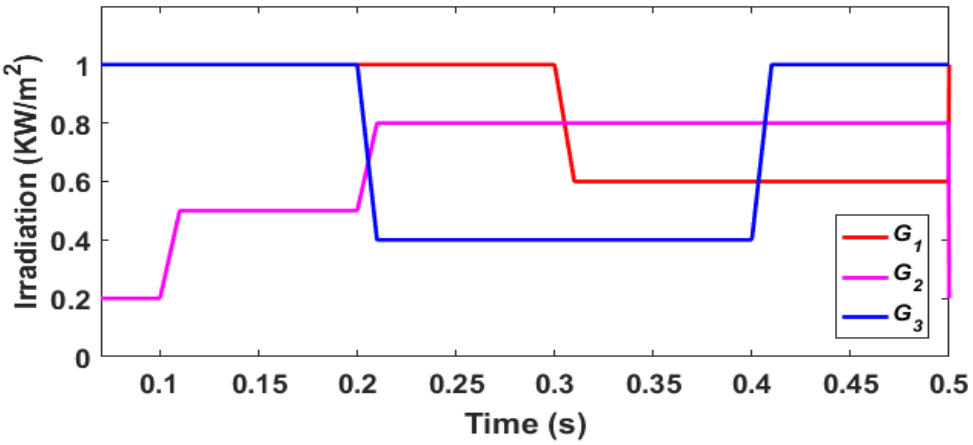

Fig. 12: Solar radiation variation in the system simulation

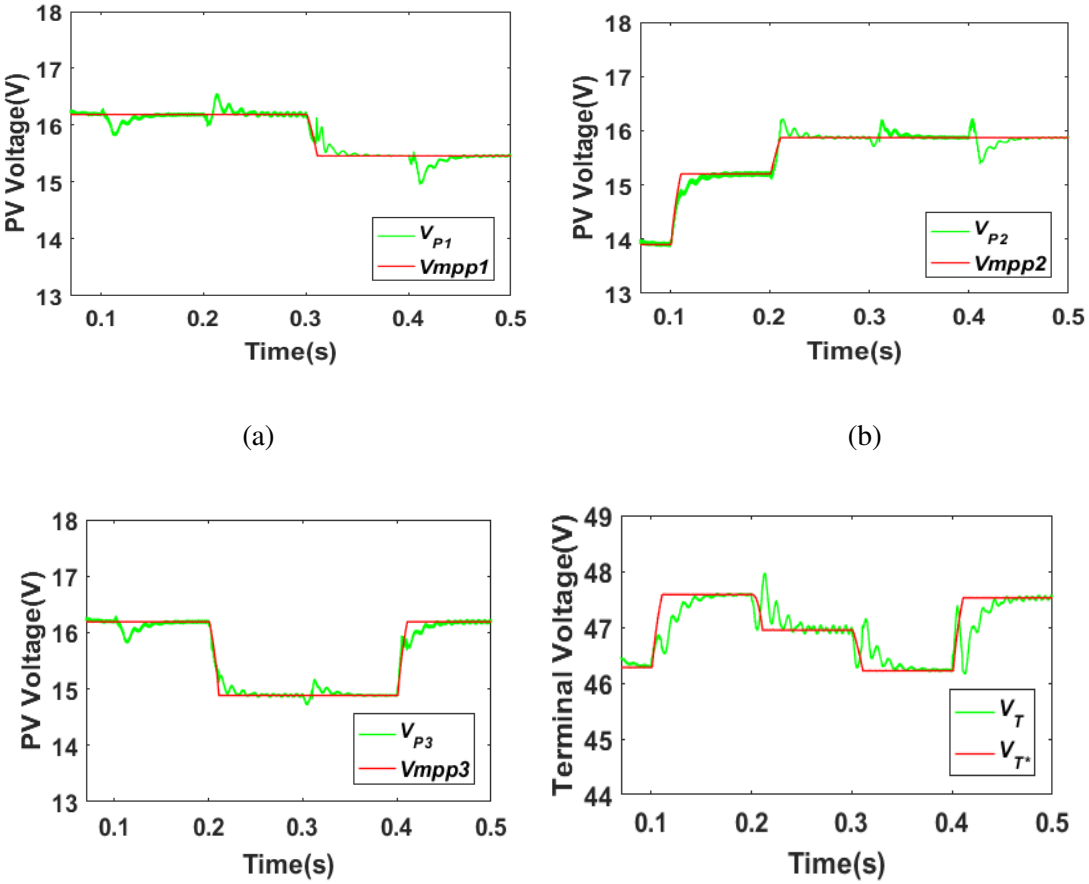

Fig. 13: Simulated voltage responses and their MPP voltages by the proposed configuration scheme with DWSSA method: (a) PV_1 panel, (b)PV_2 panel, (c) PV_3 panel and (d) input terminal voltage of boost converter

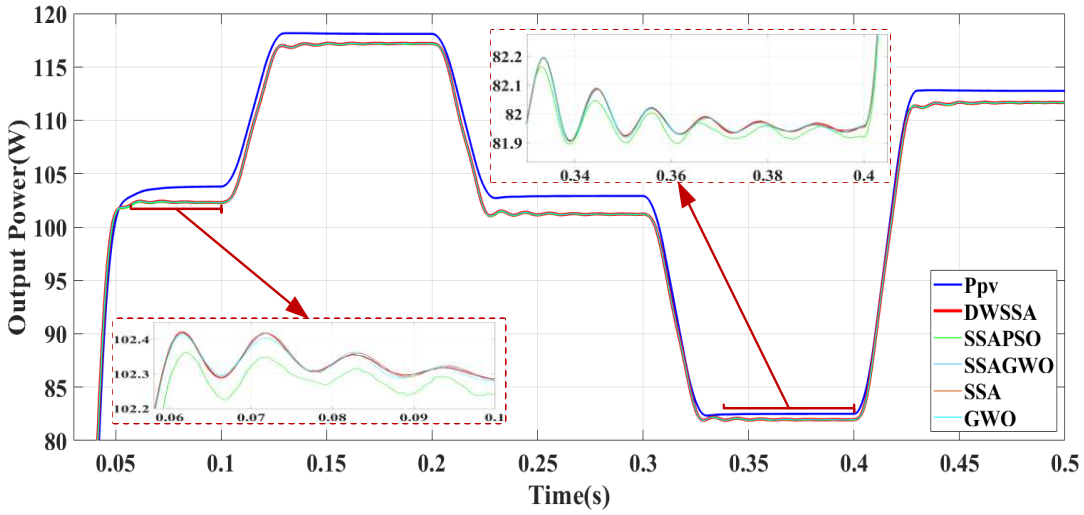

Fig. 14: Simulated total power delivered to the load, including sum of maximum power values found from the three PV sources (Ppv), DWSSA, SSAPSO, SSAGWO, SSA and GWO methods

Table 5 Simulated total power delivered to the load by 5 methods under the five cases

Method	Case (s)	0-0.1	0.1-0.2	0.2-0.3	0.3-0.4	0.4-0.5
	P_{pv}(W)	103.7	118.1	102.9	82.5	112.8
GWO	Power(W)	102.3	117.2	101.2	81.94	111.6
	Efficiency (%)	98.64	99.23	98.34	99.35	98.93
	Time (s)	0.06	0.04	0.04	0.04	0.03
SSA	Power(W)	102.4	117.1	101.3	82.0	111.6
	Efficiency (%)	98.74	99.15	98.44	99.39	98.93
	Time (s)	0.06	0.04	0.04	0.04	0.04
SSAGWO	Power(W)	102.4	117.0	101.1	81.97	111.5
	Efficiency (%)	98.74	99.06	98.25	99.35	98.84
	Time (s)	0.06	0.04	0.04	0.04	0.04
SSAPSO	Power(W)	102.2	117.0	101.3	81.95	111.7
	Efficiency (%)	98.55	99.06	98.44	99.33	99.02
	Time (s)	0.07	0.04	0.04	0.04	0.03
DWSSA	Power(W)	102.4	117.2	101.3	81.97	111.6
	Efficiency (%)	98.74	99.23	98.44	99.35	98.93
	Time (s)	0.06	0.03	0.04	0.03	0.03

7 Conclusions

The technical impact of this work lies in proposing a practically realizable approach to achieve the maximum output power from a group of PV arrays when they are partially shaded. In detail the paper presented a novel DWSSA-based maximum power point estimation algorithm applied to a particular PV-converter system to search for all PV panels' maximum power voltages according to their weather conditions. The PV-converter integrated system consists of multiple PV-Ćuk converter modules connected in a series chain with a terminal step-up converter for load connection. The SSA estimated MPP voltages were used as the reference values in the two-loop feedback control scheme for each PVCC module in a system. The simulation study performed on a PV system formed by two PVCC modules and three PV panels has shown that the terminal voltages of all PV panels can track closely to the DWSSA predicted MPP voltages with accuracy and minimum oscillation. The total voltage of the whole system, i.e. the input voltage of the terminal boost converter has been shown to be the sum of the individual PV panel's MPP voltages, and the total power is the sum of the individual powers under all three different irradiation levels. The work demonstrated that the proposed configuration and control scheme enabled individual PV panel to track their respective MPPs and hence achieve total system MPP generation. Thus, the technical impact of this project is in proposing one practically realizing approach to achieving the maximum output power from PV arrays when they are partially shaded and module mismatching.

Acknowledgements

This work has been supported by the China Postdoctoral Science Foundation (Grant No. 2018M643410), the Chongqing Special Postdoctoral Science Foundation (Grant No. XmT2018033), the Natural Science Foundation of Chongqing, China (Grant No. cstc2019jcyj-bshX0047), the National Natural Science Foundation of China (Grant No. 51707026) and the National Key Research and Development Program (Grant No. 2018YFB0905802).

List of Symbols and Abbreviations

A_o: Solar cell ideality factor;

q :Electronic charge;

K_o: Boltzmann constant;

R_p: Solar cell parallel resistance;

R_s: Solar series resistance representing ohmic loss;

SSA: Salp swarm algorithm;

DWSSA: SSA with dynamic w factor;

MPPT: Maximum power point tracking;

DMPPT: Distributed maximum power point tracking;

GMPP: Global maximum power point;

MPPs: Maximum power points;

PV: Photovoltaic;

PVCC: PV-Ćuk converter.

References

Amir, A., Amir, A., Che, H. S., Elkhateb, A., Abd Rahim, N., 2019. Comparative analysis of high voltage gain DC-DC converter topologies for photovoltaic systems. Renew. energy 136, 1147-1163.

Alharbi, B. M., Alhomim, M. A., McCann, R. A., 2020. A High Voltage Ratio Three-stage Cascaded Interleaved Boost Converters for PV Application. In 2020 IEEE Power and Energy Conference at Illinois (PECI), 1-5.

Ali, I.R., Ewees, A.A., Diego, O., Mohamed, A.E., Li S.F., 2018. Improved salp swarm algorithm based on particle swarm optimization for feature selection. J. Amb. Intel. Hum. Comp.

Abdalla, I., Corda, J., Zhang, L., 2012. Multilevel DC-link inverter and control algorithm to overcome the PV partial shading. IEEE Trans. Power Electron. 28(1), 14-18.

Bingöl, O., Özkaya, B., 2018. Analysis and comparison of different PV array configurations under partial shading conditions. Sol. Energy 160, 336-343.

Belhachat, F., Larbes, C., 2019. Comprehensive review on global maximum power point tracking techniques for PV systems subjected to partial shading conditions. Sol. Energy 183, 476-500.

Boztepe, M., Guinjoan, F., Velasco-Quesada, G., Silvestre, S., Chouder, A., Karatepe, E., 2013. Global MPPT scheme for photovoltaic string inverters based on restricted voltage window search algorithm. IEEE Trans. Ind. Electron. 61(7), 3302-3312.

Bratcu, A. I., Munteanu, I., Bacha, S., Picault, D., Raison, B., 2010. Cascaded dc–dc converter photovoltaic systems: Power optimization issues. IEEE Trans. Ind. Electron. 58(2), 403-411.

Babu, S. M., Narasimharaju, B. L., 2020. Single-phase boost DC-link integrated cascaded multilevel inverter for PV applications. IET Power Electron..

Bishop, J. W., 1988. Computer simulation of the effects of electrical mismatches in photovoltaic cell interconnection circuits. Sol. C. 25(1), 73-89.

Chen, X., Pise, A. A., Elmes, J., Batarseh, I., 2019. Ultra-highly efficient low-power bidirectional cascaded buck-boost converter for portable PV-battery-devices applications. IEEE Trans. Indus. Appl. 55(4), 3989-4000.

Chong, B. V. P., Zhang, L., 2013. Controller design for integrated PV–converter modules under partial shading conditions. Sol. Energy 92, 123-138.

Du, Y., Lu, D. D. C., 2011. Battery-integrated boost converter utilizing distributed MPPT configuration for photovoltaic systems. Sol. Energy 85(9), 1992-2002.

Femia, N., Lisi, G., Petrone, G., Spagnuolo, G., Vitelli, M., 2008. Distributed maximum power point tracking of photovoltaic arrays: Novel approach and system analysis. IEEE Trans. Ind. Electron. 55(7), 2610-2621.

Ghaderi, D. 2019. A Multi-Level DC-DC Converter Configuration for PV Applications. In 2019 11th International Conference on Electrical and Electronics Engineering (ELECO) (pp. 225-229). IEEE.

Gallardo-Saavedra, S., Karlsson, B., 2018. Simulation, validation and analysis of shading effects on a PV system. Sol. Energy 170, 828-839.

Hossain, M. Z., Jeyraj, A., Selvaraj, L., Rahim, N. A., 2018. High voltage-gain full-bridge cascaded dc-dc converter for photovoltaic application. Plos One 13(11), e0206691.

Kadri, R., Gaubert, J. P., Champenois, G., 2011. Nondissipative string current diverter for solving the cascaded DC–DC converter connection problem in photovoltaic power generation system. IEEE Trans. on Power Electron. 27(3), 1249-1258.

Kajihara, A., Harakawa, A. T., 2005. Model of photovoltaic cell circuits under partial shading. In 2005 IEEE International Conference on Industrial Technology (pp. 866-870). IEEE.

Kermadi, M., Berkouk, E. M., 2017. Artificial intelligence-based maximum power point tracking controllers for Photovoltaic systems: Comparative study. Renew. Sustain. Energy Rev. 69, 369-386.

Mao, M., Cui, L., Zhang, Q., Guo, K., Zhou, L., Huang, H., 2020. Classification and summarization of solar photovoltaic MPPT techniques: A review based on traditional and intelligent control strategies. Energy Rep. 6, 1312-1327.

Mirza, A., Mansoor, M., Ling, Q., Yin, B., Javed, M., 2020. A Salp-Swarm Optimization based MPPT technique for harvesting maximum energy from PV systems under partial shading conditions. Energy Convers. Manage. 209, 112625.

Mao, M., Zhang, L., Duan, P., Duan, Q., Yang, M.， 2018. Grid-connected modular PV-Converter system with shuffled frog leaping algorithm based DMPPT controller. Energy 143, 181-190.

Munoz, M. A., Alonso-García, M. C., Vela, N., Chenlo, F., 2011. Early degradation of silicon PV modules and guaranty conditions. Sol. Energy 85(9), 2264-2274.

Mohamed, M. A., Diab, A. A. Z., Rezk, H., 2019. Partial shading mitigation of PV systems via different meta-heuristic techniques. Renew. energy 130, 1159-1175.

Mirjalili, S., Gandomi, A. H., Mirjalili, S. Z., Saremi, S., Faris, H., & Mirjalili, S. M., 2017. Salp Swarm Algorithm: A bio-inspired optimizer for engineering design problems. Adv. Eng. Softw. 114, 163-191.

Mohanty, S., Subudhi, B., Ray, P.K., 2015. A new MPPT design using grey wolf optimization technique for photovoltaic system under partial shading conditions. IEEE Trans. Sustain. Energy 7(1), 181-188.

Noguchi, T., Togashi, S., Nakamoto, R., 2002. Short-current pulse-based maximum-power-point tracking method for multiple photovoltaic-and-converter module system. IEEE Trans. Ind. Electron. 49(1), 217-223.

Schaef, C., Stauth, J. T., 2014. Multilevel power point tracking for partial power processing photovoltaic converters. IEEE J. Em. Sel. Top. Power Electron. 2(4), 859-869.

Tatabhatla, V. M. R., Agarwal, A., Kanumuri, T., 2019. Performance enhancement by shade dispersion of Solar Photo-Voltaic array under continuous dynamic partial shading conditions. J. Clean. Prod. 213, 462-479.

Urtasun, A., Lu, D. D. C., 2015. Control of a single-switch two-input buck converter for MPPT of two PV strings. IEEE Trans. Ind. Electron. 62(11), 7051-7060.

Upadhyay, P., Kumar, R., 2019. A high gain cascaded boost converter with reduced voltage stress for PV application. Sol. Energy 183, 829-841.

Verdugo, C., Kouro, S., Rojas, C. A., Perez, M. A., Meynard, T., Malinowski, M., 2019. Five-level T-type cascade converter for rooftop grid-connected photovoltaic systems. Energies 12(9), 1743.

Woyte, A., Nijs, J., Belmans, R., 2003. Partial shadowing of photovoltaic arrays with different system configurations: literature review and field test results. Sol. Energy 74(3), 217-233.

Walker, G. R., Sernia, P. C., 2004. Cascaded DC-DC converter connection of photovoltaic modules. IEEE Trans. on Power Electron. 19(4), 1130-1139.

Wan Y., Mao M., Zhou L., 2019. A Novel Nature-Inspired Maximum Power Point Tracking (MPPT) Controller Based on SSA-GWO Algorithm for Partially Shaded Photovoltaic Systems. Electron. 8(6), 680.

Yang, B., Zhong, L., Zhang, X., Shu, H., Yu, T., Li, H., Sun, L., 2019. Novel bio-inspired memetic salp swarm algorithm and application to MPPT for PV systems considering partial shading condition. J. Clean. Prod. 215, 1203-1222.

Zhang, X., Hu, Y., Mao, W., Zhao, T., Wang, M., Liu, F., Cao, R., 2020. A Grid-Supporting Strategy for Cascaded H-Bridge PV Converter Using VSG Algorithm with Modular Active Power Reserve. IEEE Trans. Ind. Electron..

Zhuang, Y., Liu, F., Huang, Y., Zhang, X., Zha, X., 2019. A Voltage-Balancer-Based Cascaded DC–DC Converter With a Novel Power Feedforward Control for the Medium-Voltage DC Grid Interface of Photovoltaic Systems. IEEE Access 7, 178094-178107.